Molecular Therapy
Original Article

Development of a peptide drug restoring AMPK and adipose tissue functionality in cancer cachexia

Honglei Ji,[1,2,3,11] Felix Englmaier,[3,4,5,11] Pauline Morigny,[1,2,3] Maude Giroud,[1,2,3] Pamina Gräsle,[1,2,3] Sebastian Brings,[6,7] Julia Szendrödi,[6] Mauricio Berriel Diaz,[1,2,3] Oliver Plettenburg,[3,4,5,8,9,12] Stephan Herzig,[1,2,3,10,12] and Maria Rohm[1,2,3,12]

[1]Institute for Diabetes and Cancer, Helmholtz Diabetes Center, Helmholtz Center Munich, 85764 Neuherberg, Germany; [2]Joint Heidelberg-IDC Translational Diabetes Unit, Heidelberg University Hospital, 69120 Heidelberg, Germany; [3]German Center for Diabetes Research (DZD), 85764 Neuherberg, Germany; [4]Institute of Medicinal Chemistry, Molecular Targets and Therapeutics Center, Helmholtz Center Munich, 85764 Neuherberg, Germany; [5]Institute of Organic Chemistry, Center of Biomolecular Research, Leibniz University Hannover, 30167 Hannover, Germany; [6]Department of Internal Medicine I and Clinical Chemistry, Joint Heidelberg-IDC Translational Diabetes Unit, Heidelberg University Hospital, 69120 Heidelberg, Germany; [7]Department of Nuclear Medicine, University Hospital Heidelberg, 69120 Heidelberg, Germany; [8]Laboratory of Nano- and Quantum Engineering (LNQE), Leibniz University Hannover, 30167 Hanover, Germany; [9]Institute of Lung Health (ILH), 35392 Gießen, Germany; [10]Chair Molecular Metabolic Control, Technical University Munich, 81675 Munich, Germany

Cancer cachexia is a severe systemic wasting disease that negatively affects quality of life and survival in patients with cancer. To date, treating cancer cachexia is still a major unmet clinical need. We recently discovered the destabilization of the AMP-activated protein kinase (AMPK) complex in adipose tissue as a key event in cachexia-related adipose tissue dysfunction and developed an adeno-associated virus (AAV)-based approach to prevent AMPK degradation and prolong cachexia-free survival. Here, we show the development and optimization of a prototypic peptide, Pen-X-ACIP, where the AMPK-stabilizing peptide ACIP is fused to the cell-penetrating peptide moiety penetratin via a propargylic glycine linker to enable late-stage functionalization using click chemistry. Pen-X-ACIP was efficiently taken up by adipocytes, inhibited lipolysis, and restored AMPK signaling. Tissue uptake assays showed a favorable uptake profile into adipose tissue upon intraperitoneal injection. Systemic delivery of Pen-X-ACIP into tumor-bearing animals prevented the progression of cancer cachexia without affecting tumor growth and preserved body weight and adipose tissue mass with no discernable side effects in other peripheral organs, thereby achieving proof of concept. As Pen-X-ACIP also exerted its anti-lipolytic activity in human adipocytes, it now provides a promising platform for further (pre)clinical development toward a novel, first-in-class approach against cancer cachexia.

INTRODUCTION

Cachexia is the deadly outcome of many late-stage cancers. Severe wasting of adipose tissue and muscle mass, insulin resistance, cardiac dysfunction, and systemic inflammation characterize the disease. Depending on the tumor type, up to 80% of patients show symptoms, and 30% of all patients with cancer will die of cachexia.[1–4] In 2020, the International Agency for Research on Cancer estimated that new cancer cases and cancer deaths rose to 19.3 and 10 million, respectively (IARC Press Release 292), i.e., cachexia accounts for 3 million deaths per year, worldwide. In earlier stages, cachexia negatively affects quality of life and treatment success of the underlying tumor. To date, no efficient treatment against wasting is available. Hence, we are facing a critical unmet and urgent medical need of developing treatment options.

Both too much (obesity) and too little (lipodystrophy, wasting) adipose tissue are detrimental for health.[5] Adipose tissues are major metabolic organs, not only as energy storage sites but also by secreting adipokines and regulating whole-body energy homeostasis. AMP-activated protein kinase (AMPK) is an energy sensor that detects deficits in the cellular energy status in the form of increases in the AMP/ADP-to-ATP ratio, thus being activated. Once activated, the main role of AMPK is to maintain energy homeostasis by stimulating metabolic pathways of energy production and inhibiting pathways of energy consumption, thereby preserving ATP. AMPK is a central regulator of lipid metabolism in multiple tissues including the adipose

Received 28 March 2023; accepted 30 June 2023;
https://doi.org/10.1016/j.ymthe.2023.06.020.

[11]These authors contributed equally

[12]These authors contributed equally

Correspondence: Oliver Plettenburg, Institute of Medicinal Chemistry, Molecular Targets and Therapeutics Center, Helmholtz Center Munich, 85764 Neuherberg, Germany.
E-mail: oliver.plettenburg@helmholtz-munich.de
Correspondence: Stephan Herzig, Institute for Diabetes and Cancer, Helmholtz Diabetes Center, Helmholtz Center Munich, 85764 Neuherberg, Germany.
E-mail: stephan.herzig@helmholtz-munich.de
Correspondence: Maria Rohm, Institute for Diabetes and Cancer, Helmholtz Diabetes Center, Helmholtz Center Munich, 85764 Neuherberg, Germany.
E-mail: maria.rohm@helmholtz-munich.de

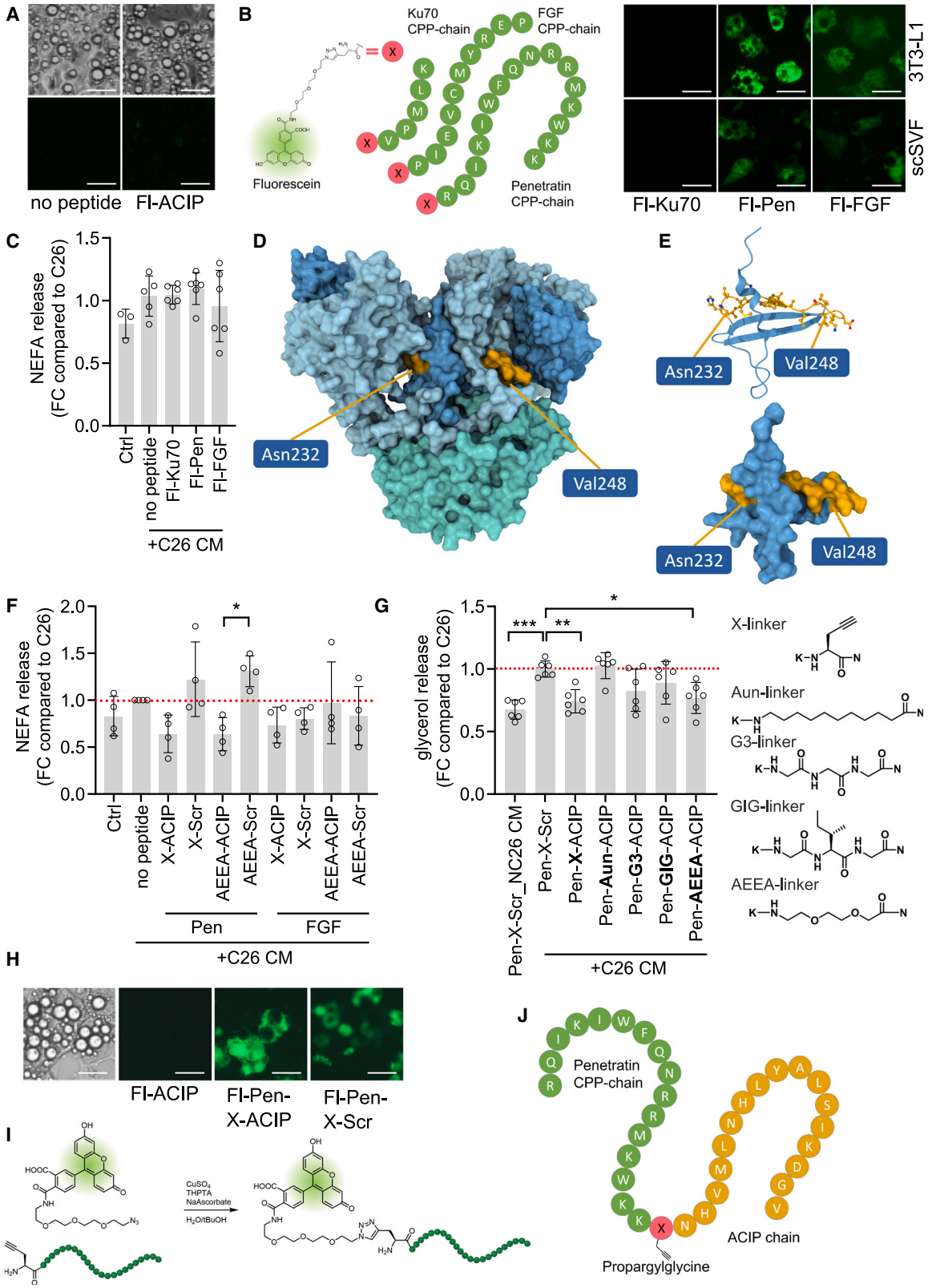

(legend on next page)

by regulating the activity of acetyl-coA carboxylase 1 and 2 (ACC1 and -2; encoded by *ACACA* and *ACACB*) through phosphorylation.[6] In addition, AMPK has been implicated in regulating lipolysis in adipose tissue: mice lacking the gene encoding the beta 1 subunit of AMPK (*Prkab1*$^{-/-}$ mice) show reduced adipose tissue mass and tend to have elevated levels of circulating fatty acids, suggestive of enhanced lipid breakdown.[7] Chronic AMPK activation has previously been linked with anti-lipolytic effects in rodents,[8] regulates the activities of key lipolytic enzymes,[9,10] and inhibits lipolysis in patients with type 2 diabetic.[11] While AMPK is typically activated in conditions of elevated lipolysis, somewhat questioning the inhibitory role of AMPK for that process,[12] the observation that anti-diabetic drugs of the biguanide and thiazolidinedione families inhibit lipolysis in an AMPK-dependent manner in human adipocytes[13] supports the concept of lipid mobilization through AMPK inhibition under certain conditions. In line, we have previously identified and successfully targeted an AMPK-dependent mechanism by which adipose tissue is lost in cachexia. Briefly, we discovered that the aberrant interaction between the lipid droplet-associated protein cell death-inducing DFFA-like effector A (CIDEA) and AMPK, as previously described in brown adipose tissue,[14] leads to AMPK degradation in cachectic white adipose tissue (WAT). This is associated with elevated adipocyte lipolysis *in vitro* and *in vivo* in mice with cachexia. Blocking this interaction with a virus coding for the peptide sequence of amino acids 232–248 of AMPKβ1 prevents AMPK from degradation. We termed this peptide sequence AMPK-CIDEA interfering peptide (ACIP). Treating tumor-bearing mice with the virus encoding the ACIP sequence prevents adipose tissue loss and prolongs cachexia-free survival.[15]

Building on our previous results, we here aimed to develop a peptide-based drug to counteract adipocyte dysfunction and cachexia *in vivo*. Using tumor-induced adipocyte lipolysis (as assessed by glycerol and/or non-esterified fatty acid release) as a screening tool, we developed novel peptides consisting of 3 moieties for optimized *in vivo* usage: (1) a cell-penetrating peptide moiety for optimized virus-free uptake into adipocytes, (2) a chemical linker, and (3) the peptide sequence of amino acids 232–248 of AMPKβ1, ACIP. Having demonstrated successful peptide application in cachectic mice and human adipocytes, we have developed a peptide-based cachexia drug targeting adipose tissue lipid homeostasis, with potential for further drug development in patients.

RESULTS

Generation and validation of ACIP-derived peptides

Having previously established virus-mediated uptake of the ACIP peptide sequence into adipocytes,[15] we here aimed to develop a virus-free translational targeting approach. ACIP peptide uptake into adipocytes was poor without the addition of any transfection reagent as shown by the low fluorescent signal of 3T3-L1 adipocytes treated with 5 μg/mL fluorescently labeled ACIP (Fl-ACIP) (Figure 1A). Thus, in order to generate a virus-free delivery method, we took advantage of cell-penetrating peptides (CPPs), were well documented to deliver peptides into cells.[16,17] The broader group of CPPs can be categorized along several criteria such as origin of the sequence (natural vs. synthetic), physicochemical properties (hydrophobic vs. cationic vs. amphipathic), or mode of entry (direct translation vs. endocytosis).[18] To validate an initial set of candidates, we evaluated representative sequences of the respective classes with proven cell-penetrating efficacy. This led us to Ku70 as a lipophilic uncharged small CPP,[19] penetratin (Pen) as a polycationic CPP,[20] and FGF-12 as an amphipathic peptide.[21] Calculation of physicochemical parameters using CellPPD[22] ensured coverage of a diverse array of properties for the selected candidates (Table 1).

The CPPs were synthesized with an N-terminal propargylic glycine as a clickable handle for subsequent conjugation with fluorescein by copper-catalyzed azide-alkyne cycloaddition (CuAAC). This allowed straightforward visualization of their intracellular distribution in adipocytes. We found that Fl-Pen and Fl-FGF, but not Fl-Ku70, were efficiently taken up by both 3T3-L1 and stromal vascular fraction (SVF)-derived primary adipocytes (Figure 1B). We have previously observed that restoring AMPK activity in adipocytes prevents tumor-induced lipolysis.[15] In order to exclude that CPPs alone had any effect on adipocyte lipolysis, we assessed if Fl-Pen, Fl-FGF, or Fl-Ku70 influenced the release of non-esterified fatty acids from adipocytes in the presence of C26 cancer cell-conditioned medium (C26 CM). Neither of the CPPs alone influenced C26 CM-induced lipolysis (Figure 1C).

ACIP consists of 17 amino acids derived from the AMPKβ1 subunit of AMPK, position 232–248. The ACIP sequence as part of AMPKβ1 contributes to two different surface interactions within the AMPK complex: the N-terminal part (Asn232-Leu236) shows a small contribution to the protein's surface in conjunction with AMPKα

Figure 1. Generation and validation of ACIP-derived peptides

(A) Uptake of fluorescently labeled ACIP (Fl-ACIP) into 3T3-L1 adipocytes visualized after 24 h by transmitted light microscopy (top) or fluorescence (bottom). (B) Uptake of fluorescently labeled cell-penetrating peptides Fl-Ku70, Fl-Pen, and Fl-FGF in 3T3-L1 (top) or subcutaneous adipose tissue SVF-derived (bottom) adipocytes after 24 h. (C) NEFA release from SVF-derived adipocytes treated for 24 h with non-conditioned control medium (Ctrl) or C26 conditioned medium (CM) in the presence or absence of Fl-KU70, Fl-Pen, and Fl-FGF. (D) Visualization of ACIP (gold) as part of the AMPK complex. Protein surface visualized by ChimeraX from PDB: 4CFE. Light blue: AMPKα, dark blue: AMPKβ, teal: AMPKγ. Beginning and end of ACIP sequence denoted by labels. (E) Model of ACIP peptide (gold) as part of AMPKβ1 3D structure. Top: cartoon view, containing ball-and-stick models of ACIP side chains. β-Sheet conformation of C-terminal ACIP and neighboring region visible. Bottom: ACIP (gold) contributions to AMPKβ1 (dark blue) isolated surface area. (F) NEFA release from 3T3-L1 adipocytes treated 24 h with C26 CM and indicated peptides. X (propargylic glycine) and AEEA indicate different linkers. 4 independent experiments. One-way ANOVA with Tukey's multiple comparison test, *p < 0.05. (G) Glycerol release from 3T3-L1 adipocytes treated 24 h with C26 CM and indicated peptides (2.2 μM) with different linkers for the connection of penetratin with ACIP. One-way ANOVA with Dunnet's multiple comparison test, *p < 0.05, **p < 0.01, ***p < 0.001. (H) Uptake of Fl-Pen-X-ACIP and Pen-X-Scr into 3T3-L1 adipocytes. (I) Scheme of click-chemistry conjugation of Azido-PEG-fluorescein to propargyl glycine-modified CPPs. (J) Sequence schematic of lead compound Pen-X-ACIP. (A, B, and H) Scale bar, 20 μm.

Table 1. Computed physicochemical parameters of candidate CPP sequences

Name	Sequence	Hydrophobicity	Hydropathicity	Amphipathicity	Hydrophilicity	Charge
Ku70	VPMLK	0,03	0,88	0,73	−0,32	1
FGF	PIEVCMYREP	−0,15	−0,29	0,50	0,11	−1
Pen	RQIKIWFQNRRMKWKK	−0,54	−1,73	1,53	0,46	7

The selected sequences show marked differences in parameters relevant to cell penetration. This broad range of values is indicative of the diversity of selection from the wide field of known CPPs.

(Figure 1D), and the C-terminal region of ACIP (Leu242-Val248) comprises of a β-sheet structure including a loop to the next segment of the sheet (Figure 1E). This region forms a contact to both AMPKα and AMPKγ while still being exposed to solvent. Since the full structure of the proposed binding partner CIDEA is not known to date, it is not possible to exactly map the interaction site; however, our *in silico* approaches confirmed the localization of the ACIP sequence in an accessible area of the AMPK complex, supporting a role as protein-binding surface.

Since both Fl-Pen and Fl-FGF were taken up into adipocytes, we next conjugated them to either the ACIP peptide or a scrambled version of the ACIP peptide (Scr) through different amino acid linkers (propargylic glycine X and AEEA). The scrambled control was used to exclude non-sequence-specific effects due to differences in charge and overall polarity. We used cancer cell CM-induced lipolysis of 3T3-L1 adipocytes, measured by the release of glycerol or non-esterified fatty acids, as a screening tool to identify peptides most suitable for counteracting tumor-induced adipocyte wasting. We found that only Pen-linker-ACIP, but not FGF-linker-ACIP, could inhibit C26 CM-induced lipolysis compared with its scrambled control (Figure 1F). Next, to further optimize the compound potency, we tested more Pen-ACIP peptides conjugated with different linkers (X, Aun, G3, GIG, and AEEA) with the lipolysis assay. We found that Pen-X-ACIP and Pen-AEEA-ACIP were most efficient in terms of inhibiting C26 CM-induced lipolysis (Figure 1G). Since both X and AEEA linkers produced peptides that efficiently blocked lipolysis in adipocytes, and we wanted to keep the capability for late-stage modification by click chemistry, we continued with using Pen-X-ACIP. In line with ACIP-mediated AMPK activation as a driver of reduced tumor-mediated lipolysis, activation of AMPK in 3T3-L1 adipocytes using the potent small-molecule AMPK activator MK8722[23] also reduced C26 CM-induced lipolysis dose dependently, as assessed by glycerol release, and also inhibited lipopolysaccharide (LPS)-induced glycerol release (Figure S1A). Further, 5-aminoimidazole-4-carboxamide ribonucleotide (AICAR) reduced C26 CM-induced glycerol release at higher doses. The stabilization of the AMPK complex using ACIP[15] reduced the required dose of AICAR to mediate its anti-lipolytic action, as Pen-X-ACIP and AICAR co-treatment of 3T3-L1 adipocytes showed synergistic effects (Figure S1B). In addition to glycerol release, we confirmed that Pen-X-ACIP was able to enter adipocytes and that the uptake efficiencies of Pen-X-ACIP and Pen-X-Scr were comparable by visualizing a fluorescein conjugated version (Figure 1H).

In summary, we developed and optimized Pen-X-ACIP, a first-in-class peptide that is taken up by adipocytes and blocks tumor-induced lipolysis in adipocytes (Figures 1I and 1J).

Chronic exposure to glucocorticoid hormones inhibits AMPK activity in adipose tissue, thus resulting in insulin resistance.[24] In order to validate peptide functionality further before moving into animal experiments, we next tested if ACIP could restore AMPK activity and improve insulin sensitivity *in vitro* in adipocytes treated with dexamethasone. Indeed, we found that Pen-X-ACIP treatment alleviated dexamethasone-induced insulin resistance in 3T3-L1 adipocytes, as demonstrated by improved glucose uptake in Pen-X-ACIP-treated cells (Figure S1C). Further, Pen-X-ACIP, but not Pen-X-Scr, restored the ability of insulin to block isoproterenol-induced lipolysis in adipocytes rendered insulin resistant by chronic dexamethasone treatment (Figure S1D).

The 17 amino acid sequence of ACIP derived from the AMPKβ1 subunit of AMPK (position 232–248) is conserved between mouse and human. Thus, we next examined the effects of Pen-X-ACIP on human adipocytes. Fl-Pen-X-ACIP was efficiently taken up by two different human adipocyte cell lines: human mesenchymal stem cell (hMSC)-derived adipocytes (Figure 2A) and human multipotent adipose-derived stem cells (hMADSCs) (Figure 2B). Incubating hMSC-derived adipocytes with HCT116 tumor cell CM led to increased lipolysis as assessed by an increase in glycerol release. Pen-X-ACIP treatment partially restored the increased lipolysis (Figure 2C), indicating that Pen-X-ACIP could be effective in human cancer cachexia treatment.

Pen-X-ACIP is stable and reaches adipose tissues upon systemic delivery in mice

Having identified Pen-X-ACIP as a peptide that is taken up by both mouse and human adipocytes and demonstrated functionality in restoring AMPK activity at various levels *in vitro*, we next sought to move into animal models. To this end, we initially investigated the stability of the peptides. We used slightly acidic solutions due to enhanced solubility in this medium. Nuclear magnetic resonance (NMR) spectroscopy demonstrated stability of the peptides in solution over the course of 24 h (Figure S2). At an uncorrected pH (6), desired concentrations (200 μM) of the peptides could only be dissolved using 5% DMSO as a co-solvent. We observed an apparent slight decline of the concentration of Pen-X-ACIP; the original concentration could, however, be restored by slightly acidifying the

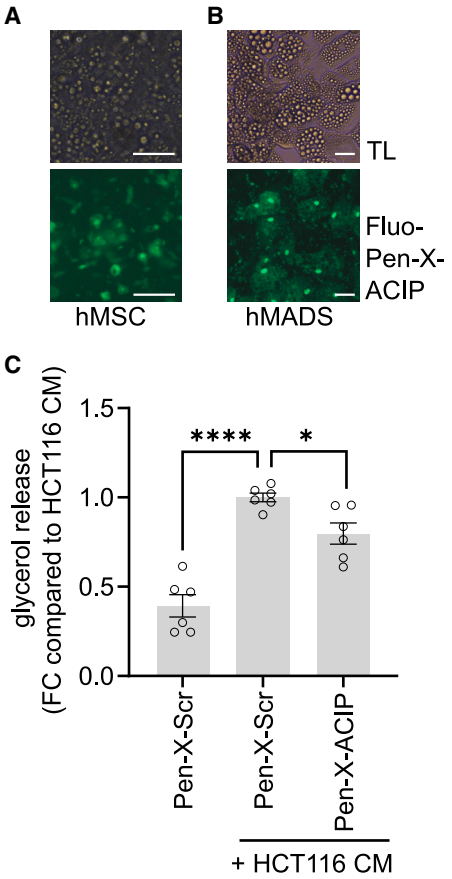

Figure 2. Pen-X-ACIP prevents cachexia-induced lipolysis in human adipocytes

Uptake of Fl-Pen-X-ACIP (4.4 μM) in hMSC- (A) or hMADSC-derived (B) adipocytes visualized after 24 h by transmitted light microscopy (top) or fluorescence (bottom). Scale bar, 10 μm. (C) Glycerol release from hMSC-derived adipocytes treated 24 h with HCT116 CM and Pen-X-ACIP or Pen-X-Scr control peptide (2.2 μM). Data are means ± SEM. One-way ANOVA with Tukey's multiple comparison test, *p < 0.05, ****p < 0.0001.

sample solution. No degradation products were detected in mass spectrometry, further indicating chemical stability of the peptide in solution. The polybasic nature of the peptides in combination with the limited solubility at the uncorrected pH suggest an equilibrium of different protomeric species in which the less protonated states might be prone to (temporary) aggregation. A twice-daily injection scheme for *in vivo* experiments was chosen as a precaution since the peptide solution might be prone to aggregation phenomena in addition to the generally shorter half-life times of peptides *in vivo* compared with small-molecule drugs. To avoid the observed effects of aggregation, solutions for *in vivo* experiments were always prepared freshly for each injection.

To initially demonstrate peptide uptake into tissues, we labeled Pen-X-ACIP with ^{68}Ga and measured body distribution upon intravenous (i.v.) and intraperitoneal (i.p.) injection by positron emission tomography (PET) imaging at different time points after injection. Upon i.v. injection, we found fast and profound uptake of the peptide into liver and kidneys. In contrast, i.p. injection resulted in patterns indicating fast uptake into abdominal adipose tissue or intestine, with only marginal uptake into liver, kidneys, or circulation (Figure 3A). To determine Pen-X-ACIP biodistribution in a more quantitative manner, we labeled Pen-X-ACIP with ^{177}Lu and measured the uptake of peptide into different tissues over a time course of 24 h. The peptide was rapidly absorbed and distributed in different metabolic organs, and the accumulation lasted for up to 24 h, depending on the tissue. With i.v. injection, the peptide predominantly accumulated in the liver and kidney. In contrast, i.p. injection resulted in a higher accumulation of peptide in abdominal WAT (aWAT), followed by clearing in the kidney (Figure 3B). Based on these uptake and stability data, we chose twice-daily i.p. injection of Pen-X-ACIP in 5% DMSO/saline as our method of choice for the mouse experiments.

Systemic Pen-X-ACIP delivery counteracts adipose tissue loss in a mouse model of cancer cachexia

We next wanted to assess the functionality of Pen-X-ACIP to counteract cancer cachexia in mice. Thus, we first excluded any effects of Pen-X-ACIP on cancer cell growth (Figure S3), as well as on liver toxicity (Figure S4). To evaluate the therapeutic potential of Pen-X-ACIP *in vivo*, we utilized an established cancer cachexia mouse model, the C26 model, by injecting C26 colon cancer cells subcutaneously into the flank region of BALB/c mice. Starting 1 week after tumor inoculation, mice were injected twice daily with 10 mg/kg Pen-X-ACIP or Pen-X-Scr for 10 days. At this time, 4 out of 8 of the Pen-X-Scr-injected animals had developed cachexia (>5% weight loss compared with peak weight at day 8 after injection). In line with our *in vitro* data showing protective effects of Pen-X-ACIP on cancer-induced wasting, none of the Pen-X-ACIP-injected mice had developed >5% weight loss at that time point (Figure 4A). On average, Pen-X-Scr-injected mice lost 6.7% weight, whereas Pen-X-ACIP-injected mice lost only 1.8% weight (not significant [ns], p = 0.1). Consistently, mice treated with Pen-X-ACIP had significantly higher final body weights compared with mice treated with Pen-X-Scr despite identical initial body weight (Figures S5A and S5B). Skeletal muscle weight was unchanged by Pen-X-ACIP treatment, but the peptide positively counteracted cardiac atrophy (Figures 4B and 4C). Moreover, adipose tissue (both inguinal WAT [iWAT] and aWAT) weights were restored by Pen-X-ACIP treatment (Figures 4D and 4E). When normalized to body weight, Pen-X-ACIP significantly improved adipose tissue but not muscle or heart weights (Figures S5C–S5E). Importantly, we did not observe any difference in tumor weight between groups, reassuring us that any improvement did not come from tumor regression (Figure 4F) but was specific to improving cachexia.

Pen-X-ACIP restores AMPK function in cachectic adipose tissue

Next, we wanted to know if the beneficial effect of Pen-X-ACIP was mediated by AMPK activation. We first checked the expression of AMPK targets phosphoenolpyruvate carboxykinase (Pepck) and solute carrier family 2 member 4 (Glut4), which are significantly

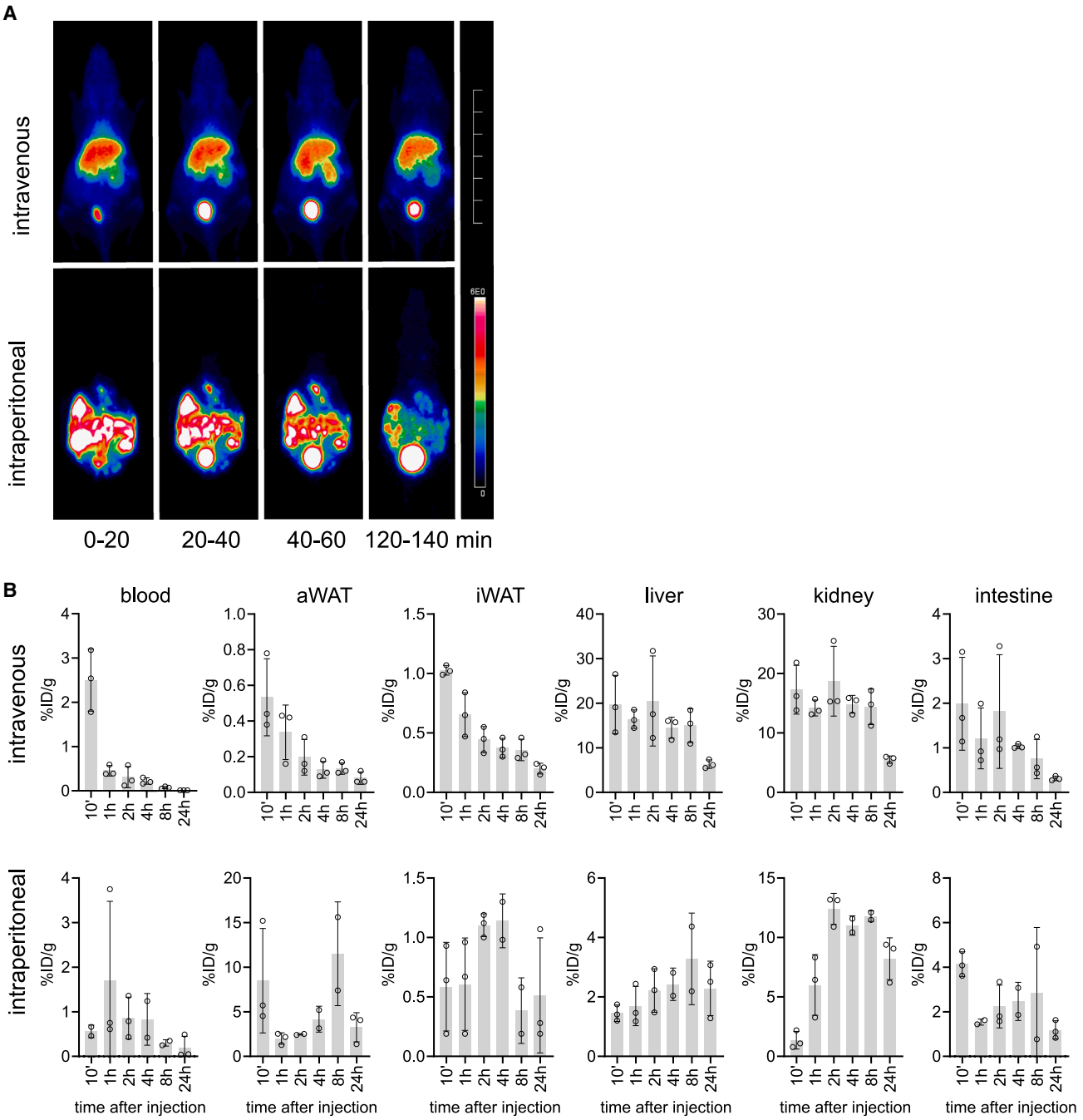

Figure 3. Pen-X-ACIP reaches the adipose tissue upon systemic delivery in mice

(A) PET imaging upon intravenous or intraperitoneal injection of ^{68}Ga-DOTA-PEN-X-ACIP. SUV images are given for indicated times between 0 and 140 min. The heatmap shows the relative intensities on a scale from 0 (black) to 6 (white). Scale bar, 60 mm. (B) Biodistribution analysis of ^{177}Lu-DOTA-PEN-X-ACIP after intravenous (top) or intraperitoneal (bottom) injection. Animals were sacrificed at indicated time points (10 min to 24 h). Values are given as the relative amount of the injected dose per gram of tissue (%ID/g) ± SD.

increased by C26-induced cachexia in aWAT (Figure 5A). In line with the described repression of Pepck and Glut4 by AMPK activation[25,26] compared with Pen-X-Scr, Pen-X-ACIP reduced the mRNA levels of both genes in the adipose tissue of C26 tumor-bearing mice (Figure 5B). In contrast, the skeletal muscle Pepck and Glut4 mRNA expression was unchanged by Pen-X-ACIP treatment (Figures S6A

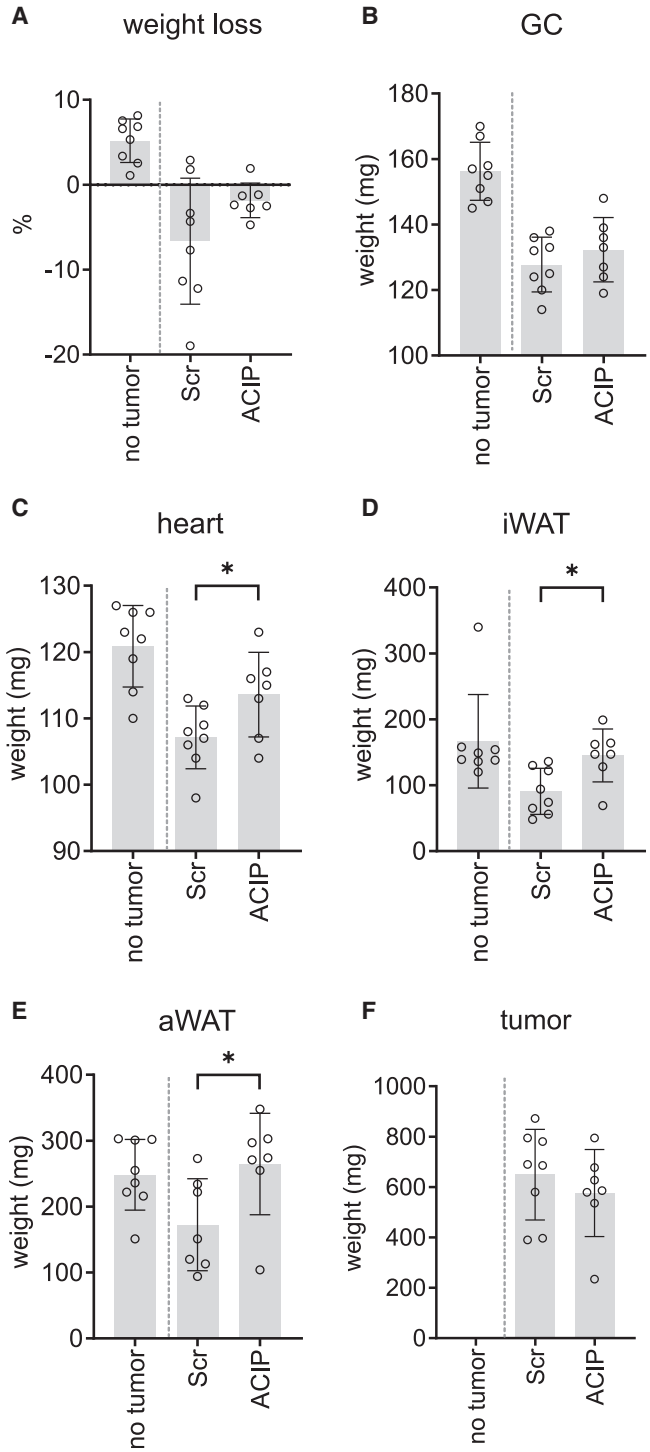

Figure 4. Pen-X-ACIP delivery counteracts adipose tissue loss in cachexia

(A–F) C26 tumor-bearing mice were injected twice daily with 10 mg/kg Pen-X-ACIP or Pen-X-Scr and killed 16 days post-injection when the majority of control animals had developed cachexia (>5% weight loss). Non-tumor-bearing animals from an independent experiment are shown as controls, separated by a dotted line. (A) Weight loss compared with initial body weight. Weights of (B) gastrocnemius muscle, (C) heart, (D) iWAT, (E) aWAT, and (F) tumor. t test *p < 0.05.

and S6B). Consistent with previous reports,[27] C26-induced cachexia increased the expression of Murf1 (muscle-specific RING finger protein 1/tripartite motif containing 63) and Atrogin1 (encoded by *Fbxo32* gene, F box protein 32) in muscle (Figure S6A). Pen-X-ACIP induced a non-significant trend to reduce expression of Murf1 and Atrogin1 in muscle (Figure S6B), in line with a trend toward improved body weight loss in Pen-X-ACIP-treated animals. Increased lipolysis in the adipose tissue is a hallmark of cancer cachexia, and reducing levels or activity of adipose triglyceride lipase (ATGL)—the key enzyme catalyzing the first step of triglyceride hydrolysis—has previously been demonstrated to counteract wasting.[28] Thus, we next assessed the expression of key genes involved in adipose tissue lipid metabolism in aWAT of Pen-X-Scr- or Pen-X-ACIP-injected cachectic mice. We found that C26-induced cachexia increased the expression of fatty acid-binding protein 4 (Fabp4) (Figure 5A). Pen-X-ACIP reduced the expression of Atgl and Fabp4 (Figure 5B), indicating that the peptide is able to counteract cachexia-induced lipolysis also *in vivo*. AMPK phosphorylates and thereby inhibits ACC, leading to reduced lipogenesis.[6,29] We have previously demonstrated that reduced ACC phosphorylation occurs in adipose tissue of cachectic mice and that increased adipocyte lipogenesis contributes to energy loss in cachexia.[15] Here, we found that Pen-X-ACIP restored ACC phosphorylation in cachectic aWAT (Figure 5C), likely by stabilizing AMPK, as the protein levels of AMPKβ1 as well as the activation (phosphorylation) of AMPKα were increased after Pen-X-ACIP treatment (Figure 5D). In contrast, Pen-X-ACIP did not affect AMPK target gene expression or activation in liver (Figures S6C and S6D).

To obtain a more systemic overview of the genes regulated by Pen-X-ACIP in aWAT, we performed RNA sequencing in aWAT of tumor-bearing mice treated with either Pen-X-ACIP or its scrambled control. We found 283 genes up-regulated and 348 genes down-regulated in Pen-X-ACIP-treated aWAT. Using gene set enrichment analysis (GSEA), we identified the interferon γ response pathway as negatively correlated with Pen-X-ACIP treatment (NES −1.783, q = 0.001), indicating that Pen-X-ACIP improved the adipose tissue inflammation commonly observed in cachectic adipose tissue. In addition, Myc targets were also negatively enriched after Pen-X-ACIP treatment (NES −1.94, q < 0.001). mTORC1 signaling, which is an important anabolic pathway antagonizing catabolic AMPK signaling, was also negatively enriched in the Pen-X-ACIP-treated adipose tissue (NES −1.2, q = 0.27), further indicating improved AMPK functionality after Pen-X-ACIP-mediated AMPK activation in cachectic adipose tissue (Figure 5E).

DISCUSSION

AMPK forms heterotrimeric complexes comprising catalytic α-subunits (α1/α2), regulatory β-subunits (β1/β2), and γ-subunits (γ1/γ2/γ3) in eukaryotic cells. They can assemble into at least 12 different heterotrimeric combinations, which can function and behave quite differently. Here, we demonstrate that ACIP stabilizes AMPKβ1, the isoform that is predominately expressed in adipose tissue, and activates AMPK in adipose tissue. AMPKβ1 is well conserved between

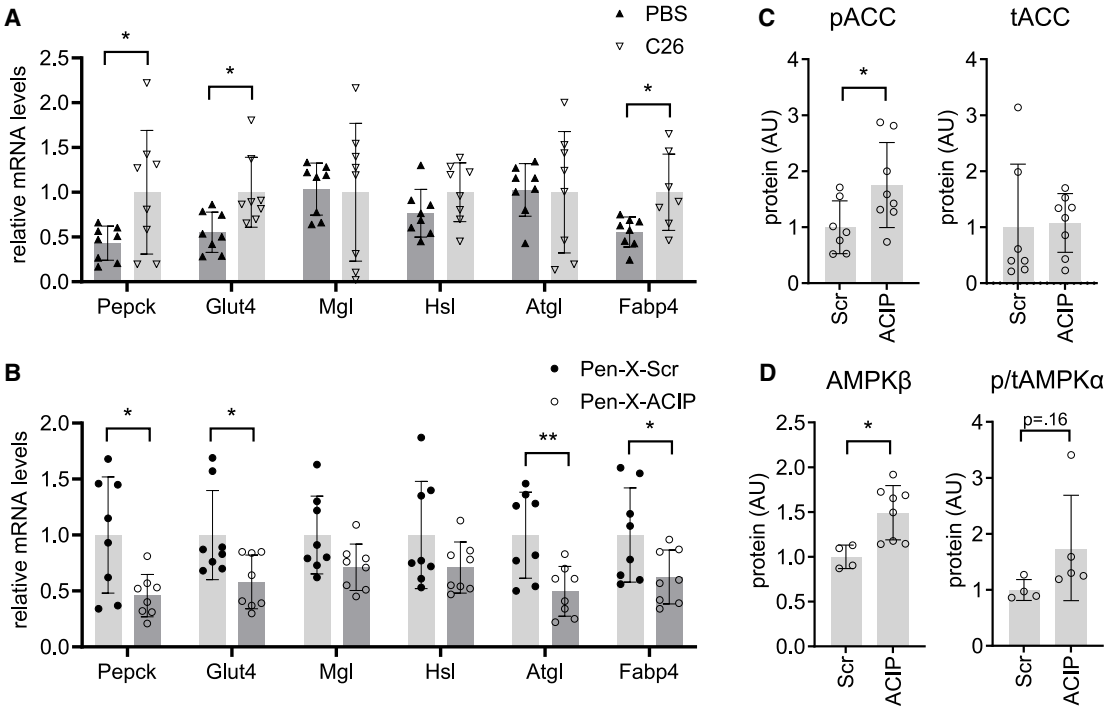

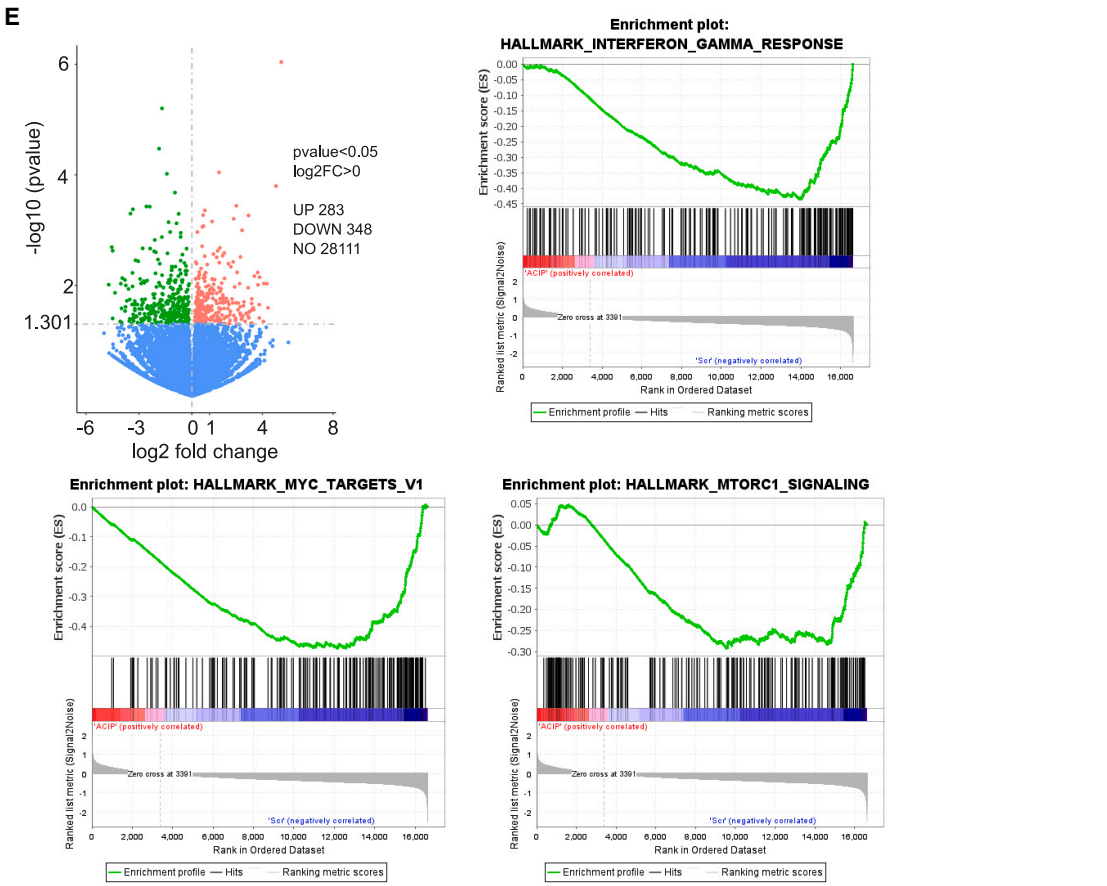

(legend on next page)

mouse and human. We also provide evidence that ACIP is effective in human adipocytes, reassuring us of the translational potential of the peptide drug approach. AMPK β1 and β2 isoforms share 71% identical sequence. The corresponding ACIP amino acid (aa) sequence on AMPK β2 differs only in one aa (247 G to S). However, whether a modified ACIP containing this altered amino acid also stabilizes the AMPK complex needs to be further validated.

Here, we provide evidence that Pen-X-ACIP preserves AMPK activity, thus inhibiting lipolysis as illustrated by decreased glycerol and NEFA release in tumor cell CM-treated mouse and human adipocytes. AMPK is an energy sensor that regulates all aspects of metabolism, from carbohydrate and fatty acid to amino acid metabolism, and also organelle (mitochondrial and lysosome) function.[30] It still needs to be determined how precisely these organelle functions and metabolic processes are altered in cachectic adipose tissues and if restoration of AMPK function by Pen-X-ACIP can reverse this metabolic dysfunction in cancer cachexia.

Many chemical AMPK activators have been developed to treat different metabolic diseases; however, undesirable side effects have been reported, e.g., MK-8722, a potent pan-AMPK activator, caused cardiac hypertrophy in mice and rhesus monkeys.[23] The molecular mechanism of ACIP function relies on the blockage of AMPKβ1 degradation in adipose tissues, at least in part through blocking the interaction of CIDEA and AMPKβ1.[14,15] Since CIDEA is a lipid droplet-associated protein predominately expressed in adipose tissues, and aberrantly upregulated in cachectic adipose tissues,[31] ACIP acts through a disease-relevant mechanism unique to adipose tissue, avoiding undesired side effects. In agreement with this, the slightly increased heart mass after ACIP treatment observed in our cachexia model is likely a phenotype of improved cachexia rather than cardiac hypertrophy related to systemic AMPK activation, as we observed no AMPK activation in muscle. Further, the heart weights of the tumor-bearing, Pen-X-ACIP-treated animals in the current study are similar to the heart weights of non-tumor-bearing BALB/c mice of the same age and vendor, as we reported previously,[32] and the fold change relates more to a reversal of cachexia-induced atrophy than hypertrophy as reported in Myers et al.[23] This is further supported by the non-significant change in heart weight when normalized to body weight (Figure S5D).

Cancer cachexia was defined as "a multifactorial syndrome characterized by an ongoing loss of skeletal muscle mass (with or without loss of fat mass) that cannot be fully reversed by conventional nutritional support and leads to progressive functional impairment."[33] Recently, adipose tissues wasting has become increasingly recognized as a hallmark of cancer cachexia.[34,35] Indeed, a substantial portion of weight loss in patients with cancer derives from the depletion of adipose tissue, attributing to increased lipolysis.[36,37] Latest cohort studies revealed distinct clinical subtypes of cachexia, demonstrating different patterns of tissue loss involving adipose and/or muscle tissues,[38] and fat loss was strongly associated with poor survival.[39] Understanding these subtypes of cachexia is crucial for tailored disease management approaches. In that regard, studying the therapeutic potential of PenX-ACIP *in vivo* in a mouse model of cancer cachexia, we found that Pen-X-ACIP treatment not only reversed the adipose tissue wasting but also reduced body weight loss in C26 tumor-bearing mice. The beneficial effects of Pen-X-ACIP were primarily mediated by the restoration of AMPK activity in cachectic adipose tissue as demonstrated by qPCR, western blot, and RNA sequencing (RNA-seq) analysis. Decreased AMPK activity has also been observed in adipose tissues of other metabolic diseases, e.g., insulin resistance and type 2 diabetes. Further experiments are needed to validate if ACIP can also stabilize and activate AMPK in adipose tissues in this context.

Overall, we demonstrate that a peptide-based drug can effectively enter adipocytes and improve cancer-induced adipose tissue wasting by targeting AMPK *in vivo*, thereby producing a peptide-based anti-cachexia drug. Given the current lack of treatment options for cachexia, our study provides the basis for further clinical development of ACIP-based peptide drugs.

MATERIALS AND METHODS

Mice

All animal studies were conducted in accordance with German animal welfare legislation. Male BALB/c and C57BL6/J mice obtained from the Charles River Laboratories were maintained in a climate-controlled environment (22°C–24°C, ∼50% humidity) with specific pathogen-free conditions under 12 h dark-light cycles (6 a.m. to 6 p.m.) in the animal facility of the Helmholtz Center Munich. Female Swiss mice obtained from Janvier Labs (Le Genest-Saint-Isle, France) were maintained in a controlled environment under 12 h dark-light cycles in the animal facility of the Department of Nuclear Medicine at the Heidelberg University Hospital. Protocols were approved by the institutional animal welfare officer, and the necessary licenses were obtained from the state ethics committee and government of Upper Bavaria (ROB-55.2-2532.Vet_02-16-13, ROB-55.2-2532.Vet_02-18-93) and Baden Wuerttemberg (35–9185.81/G-111/16). Mice were fed *ad libitum* with regular rodent chow. Mice were injected with $0.5*10^6$ C26 colon carcinoma cells in PBS subcutaneously into the right flank. Tumor growth and body weight were measured daily

Figure 5. Pen-X-ACIP restores AMPK function in cachectic adipose tissue

mRNA expression in epididymal adipose tissue of C26 tumor-bearing mice compared with tumor-free mice (A) and in C26 tumor-bearing mice treated with 10 mg/kg Pen-X-ACIP or Pen-X-Scr (B). t test *$p < 0.05$, **$p < 0.01$. (C) Protein levels of phosphorylated and total ACC relative to vinculin as housekeeping protein. (D) Protein levels of AMPKβ and phosphorylated/total AMPKα levels normalized to vinculin. t test *$p < 0.05$. Note that not all mice from (A) and (B) were available for protein extraction due to the limiting amount of adipose tissue in cachectic mice. (E) Volcano plot indicating differentially expressed genes in aWAT of Pen-X-Scr- or Pen-X-ACIP-treated C26 tumor-bearing animals. Blue indicates non-significantly altered genes, red/green indicates $p < 0.05$. Gene set enrichment analysis showing enriched hallmarks of interferon γ response, Myc targets, and mTORC1 signaling in Pen-X-ACIP-treated mice (indicated by negative enrichment score on Scr-treated mice).

for up to 16 days post-tumor cell injection. Pen-X-ACIP or Pen-X-Scr was dissolved in sterile 5% DMSO and PBS and injected i.p. at a dosage of 10 mg/kg in 50 μL volume twice daily at 6 a.m. and 6 p.m. starting 7 days after tumor cell injection. Mice were killed at 9–11 a.m. by cervical dislocation 16 days after tumor cell injection. Organs including tumor, liver, fat pads (iWAT; epididymal WAT/aWAT), and gastrocnemius (GC) muscles were collected, snap frozen in liquid nitrogen, and used for further analysis. In each animal experiment, mice were randomly assigned to each group, and groups were matched for body weight before start of compound injection.

PET imaging

DOTA-Pen-X-ACIP was labeled with ^{68}Ga, and PET was carried out in mice on a Siemens Inveon small-animal PET scanner (Siemens, Munich, Germany) after i.v. or i.p. injection. In short, ^{68}Ga was eluted from the generator with 0.1 M HCl into a tube containing 20 nmol of the peptide and 0.5% ascorbic acid in 0.5 M Na-acetate buffer. The mixture was incubated at pH 3.3–3.6 for 10 min at 95°C while stirring. Free ^{68}Ga was removed using C18 solid-phase extraction cartridges (Thermo Scientific, Waltham, MA, USA), and the purified product was eluted with ethanol and analyzed by high-performance liquid chromatography (HPLC) (Agilent Technologies, Santa Clara, CA, USA) coupled with a radio flow detector. Ethanol was evaporated, and the labeled peptide was reconstituted in a maximum of 10% DMSO and 5% concentrated sodium phosphate solution in saline solution. The peptide was administered to 10-week-old female Swiss mice by i.v. or i.p. injection. A dynamic scan was carried out for 60 min followed by a static scan from 120 to 140 min after application of the molecule. Images were reconstructed iteratively using the 3-dimensional maximum *a priori* ordered-subset expectation maximization. Images were converted to standardized uptake value (SUV) images, normalized for animal weight and injected dose.

Biodistribution analysis

For biodistribution analysis, DOTA-Pen-X-ACIP was labeled with ^{177}Lu. After labeling, free ^{177}Lu was removed by solid-phase extraction cartridges and the labeled peptide eluted with ethanol. Purity of the labeled peptide was confirmed by radio HPLC (Agilent Technologies) coupled with a radio flow detector. Ethanol was evaporated, and the labeled peptide reconstituted in a maximum of 10% DMSO and 5% concentrated sodium phosphate solution in saline solution. The peptide was administered to 10-week-old female Swiss mice by i.v. or i.p. injection. Animals (n = 3 for each time point) were killed 10 min, 1 h, 2 h, 4 h, 8 h, and 24 h after tracer administration. Organs were weighed and radioactivity was measured in the organs with a γ-counter (Packard Cobra Auto-Gamma, GMI, Phoenix, AZ, USA). The values are given as percentage of the injected dose per gram of tissue (%ID/g).

Cell culture

Preadipocytes from the SVF of inguinal adipose tissues of 8-week-old C57BL6/J mice, and 3T3-L1 cells (ATCC, Manassas, VA, USA) were cultured and differentiated by the addition of 1 μg/mL insulin, 0.25 μM dexamethasone, and 0.5 mM IBMX as described before.[15] Adipocytes were used 8–12 days post-differentiation. For tumor cell CM experiments, C26, SW480, HCT116 (DKFZ repository), and NC26 cells (kind gift by Dr. M. Schweiger, Graz[40]) were grown to 70% confluency in DMEM 10% FCS and 1% P/E, and then media were renewed and collected 48 h later. Medium from plates with no cells was used as control media. Media were diluted 3:1 with fresh DMEM for 24 h stimulation of adipocytes. Peptides were added to 3T3-L1 adipocytes in serum-free medium 3 h prior to addition of CM. 1 μM dexamethasone treatment for 24 h was used to render 3T3-L1 adipocytes insulin resistant. hMSCs and hMADSCs were cultured and differentiated as previously described.[41–43] Cell lines were regularly tested for mycoplasma contamination as required by in-house policies. Cell culture experiments were repeated at least 2–3 times with n $\geq$3 technical replicates each time. For the lipolysis assay, 3T3-L1 and primary adipocytes were washed three times in PBS and preincubated for 1 h in Krebs-Ringer buffer containing 3% BSA and 5 mM glucose, and lipolysis was measured in supernatant of cells treated for 2 h with the same buffer using NEFA and glycerol kits (Wako, Neuss; Sigma, Munich, Germany). In some experiments, glycerol levels were determined directly from culture media of 3T3-L1 cells. Uptake of fluorescently labeled peptides was imaged after 24 h. For glucose uptake assay, cells were stimulated with/without 1 μM insulin in the presence of 2-deoxy glucose-6-phosphate (2-DG6P) for 30 min. Glucose uptake was measured using the ab136955 kit (Abcam, Cambridge, UK) following the manufacturer's instructions.

Molecular graphics

Molecular graphics and analyses performed with UCSF ChimeraX,[44] developed by the Resource for Biocomputing, Visualization, and Informatics at the University of California, San Francisco, with support from National Institutes of Health R01-GM129325 and the Office of Cyber Infrastructure and Computational Biology, National Institute of Allergy and Infectious Diseases.

Solid-phase peptide synthesis

Peptides were generated by solid-phase peptide synthesis using Fmoc-based *in situ* neutralization chemistry. 0.1 mmol Rink 4-methylbenzhydrylamine (MBHA) resin (Novabiochem, Läufelfingen, Switzerland) was used on a Liberty Blue microwave synthesizer (CEM) by standard Fmoc methods using differential interference contrast (DIC)/Oxyma for coupling and 10% Piperazine in *N*-methylpyrrolidone (NMP) and ethanol (9:1 vol/vol) for Fmoc-N-deprotection. Completed peptidyl-resins were treated with TFA, EDT, water, and triisopropylsilane (94:2.5:2.5:1 vol/vol/vol/vol) for 3 h. The peptides were precipitated and washed with cold (0°C) diethylether, dissolved in water containing 20% acetonitrile (MeCN), and lyophilized. The following side-chain protecting groups were used for Fmoc-amino acids (Novabiochem): Arg(Pbf), Asn(Trt), Asp(tBu), Gln(Trt), Glu(tBu), His(Trt), Lys(Boc), Ser(tBu), Trp(Boc), Tyr(tBu). Peptide masses were confirmed by electrospray-TOF mass spectrometry (Waters LCT Premier, Milford, MA, USA) and purified.

Peptide sequences are as follows: Pen: RQIKIWFQNRRMKWKK; FGF: PIEVCMYREP; Ku70: VPMLK; ACIP: NHVMLNHLYALSIKDGV; Scr: LVYSGHIMKHLVADNLN.

Peptide purification

Crude peptide extracts were analyzed by analytical reverse-phase HPLC (MeCN/water, 0.1% FA) on a Waters 2795 separation module equipped with an Aeris wide-pore XB-C18 column (0.21 × 5 cm, Phenomenex). The crude extracts were purified by preparative reverse-phase HPLC (MeCN/water, 0.05% TFA) on a Jupiter Proteo column (2.1 × 25 cm, Phenomenex). Preparative fractions were analyzed for purity by analytical reverse-phase HPLC using the aforementioned methods. Peptide masses and purity were confirmed by electrospray-TOF mass spectrometry (Waters LCT Premier). Purified peptides were lyophilized and stored under inert atmosphere (argon) at −23°C.

Fluorescein labeling of peptides

Labeling of alkyne-modified peptides with fluorescein was achieved using CuAAC. Alkyne-modified peptide (5 mg) was dissolved in water/tBuOH (1 mL), and fluorescein-(3,6,9)-trioxaundecylazide (FPEGA; 20 mM in tBuOH) was added. The mixture was degassed by argon stream for 10 min under exclusion of light. Tris(3-hydroxypropyltriazolylmethyl)amin (THPTA; 50 mM in water) was added and then sodium ascorbate (NaAsc; 100 mM in water, freshly prepared) and optionally aminoguanidine hydrochloride (AMG; 50 mM in water) if the peptide contained any arginyl residues. CuSO4 (20 mM in water) was added and stirred at room temperature until analytical reverse-phase HPLC-mas spectrometry (MS) (see peptide purification) indicated complete conversion. Crude reaction mixtures were purified by flash column chromatography (FC) on a 4 g-C18 wide-pore cartridge (MeCN/water, 0.05% TFA) using an MPLC-Reveleris system from Büchi. Preparative fractions were analyzed for purity by analytical reverse-phase HPLC using the aforementioned methods. Peptide masses and purity were confirmed by electrospray-TOF MS (Waters LCT Premier). Purified peptides were lyophilized and stored under inert atmosphere (argon) at −23°C.

CuAAC-linked CPP-ACIP constructs

Azido-propionic-modified ACIP/Scr peptides (5 mg) and alkyne-modified CPP (1 equiv) were dissolved in water (1 mL), and it was degassed by argon stream for 10 min. AMG (50 mM in water, 5.0 equiv) and THPTA (50 mM in water, 2.5 equiv) were added, and then CuSO4 (20 mM in water, 2.5 equiv) and the mixture were degassed by argon stream for 5 min. Sodium ascorbate (5 equiv) was added and stirred until analytical reverse-phase HPLC indicated completeness of reaction. Crude reaction mixtures were purified by FC on a 4 g-C18 widepore cartridge (MeCN/water, 0.05% TFA) using an MPLC-Reveleris system from Büchi. Preparative fractions were analyzed for purity by analytical reverse-phase HPLC using the aforementioned methods. Peptide masses and purity were confirmed by electrospray-TOF MS (Waters LCT Premier). Purified peptides were lyophilized and stored under inert atmosphere (argon) at −23°C.

DOTA-labeled Pen-ACIP/Scr constructs

0.01 mmol Pen-ACIP/Scr-peptidyl-resins acquired by previously described Materials and methods (see solid-phase peptide synthesis) were subjected to a final coupling step using DOTA-tris(tert-Butyl ester) and DIC/Oxyma standard methods. Peptide cleavage and precipitation was performed using the aforementioned methods (see solid-phase peptide synthesis). DOTA-labeled Pen-ACIP/Scr constructs were purified and analyzed by the previously described Materials and methods (see peptide purification).

Protein analysis

Proteins were extracted from frozen organ samples or cultured adipocytes following lysis in ice-cold lysis buffer (50 mM Tris [pH 7.2], 150 mM NaCl, 1% NP-40, 0.5% Triton X-, 1 mM EDTA, 1 mM Na_3VO_4, 1 mM NaF, 1 μg/mL pepstatin A, and 1 mM DTT), and extracts were separated on 8%–16% SDS-polyacrylamide gels and blotted onto nitrocellulose membranes. Western blot assays were performed using antibodies specific for ACC (#3662), p-ACC-S79 (#3661), AMPKα (#2532), p-AMPKα-T172 (#2531), (Cell Signaling, Danvers, MA, USA), AMPKβ1 (Abcam, ab32112), vinculin (Abcam, ab129002), and goat anti-rabbit immunoglobulin G (IgG) (H + L)-HRP conjugate (Bio-Rad). Validation data are provided on the manufacturers' websites.

qPCR

RNA was extracted using Qiazol lysis reagent and the RNeasy Mini kit (Qiagen, Hilden, Germany) following the manufacturer's instructions. cDNA was produced using the High Capacity cDNA Reverse Transcription kit (Life Technologies, Carlsbad, CA, USA). qPCRs were performed on a QuantStudio 6 Flex Real-Time PCR System (Thermo Fisher) using Takyon Taqman Master Mix (Eurogentec, Seraing, Belgium) and Taqman probes (Thermo Fisher). RNA expression data were quantified according to the ΔCt method and normalized to levels of TATA-box binding protein RNA (TBP).

RNA-seq

This analysis was performed at Novogene (Cambridge, UK). RNA was extracted as described for qPCR. A total amount of 1 μg RNA per sample was used as input material for the RNA sample preparations. Sequencing libraries were generated using NEBNext UltraTM RNA Library Prep Kit for Illumina (NEB, Ipswich, MA, USA) following manufacturer's recommendations, and index codes were added to attribute sequences to each sample. Briefly, mRNA was purified from total RNA using poly-T oligo-attached magnetic beads. Fragmentation was carried out using divalent cations under elevated temperature in NEBNext First Strand Synthesis Reaction Buffer (5×). First-strand cDNA was synthesized using random hexamer primer and M-MuLV Reverse Transcriptase (RNase H-). Second-strand cDNA synthesis was subsequently performed using DNA Polymerase I and RNase H. Remaining overhangs were converted into blunt ends via exonuclease/polymerase activities. After adenylation of 3′ ends of DNA fragments, NEBNext Adaptor with hairpin loop structure was ligated to prepare for hybridization. In order to select cDNA fragments of preferentially 150–200 bp in length, the library fragments

were purified with AMPure XP system (Beckman Coulter, Beverly, CA, USA). Then, 3 μL USER Enzyme (NEB) was used with size-selected, adaptor-ligated cDNA at 37°C for 15 min followed by 5 min at 95°C before PCR. Then, PCR was performed with Phusion High-Fidelity DNA polymerase, Universal PCR primers, and Index (X) Primer. At last, PCR products were purified (AMPure XP system), and library quality was assessed on the Agilent Bioanalyzer 2100 system. The clustering of the index-coded samples was performed on a cBot Cluster Generation System using PE Cluster Kit cBot-HS (Illumina) according to the manufacturer's instructions. After cluster generation, the library preparations were sequenced on the Illumina NovaSeq platform, and 150 base paired-end reads were generated.

Data analysis

Raw data (raw reads) of FASTQ format were firstly processed through fastp. In this step, clean data (clean reads) were obtained by removing reads containing adapter and poly-N sequences and reads with low quality from raw data. At the same time, Q20, Q30, and GC content of the clean data were calculated. All the downstream analyses were based on the clean data with high quality. Reference genome and gene model annotation files were downloaded from the genome website browser (NCBI/UCSC/Ensembl) directly. Paired-end clean reads were mapped to the reference genome using HISAT2 software. Feature counts was used to count the read numbers mapped of each gene, including known and novel genes. Differential expression analysis between two groups (four biological replicates per condition) was performed using DESeq2 R package. The resulting p values were adjusted using the Benjamini and Hochberg's approach for controlling the false discovery rate (FDR). Genes with an adjusted p value <0.05 found by DESeq2 were assigned as differentially expressed. GSEA was performed using GSEA with hallmark gene sets.

Statistical analysis

Unless otherwise stated, results are presented as mean ± SD. Significance was tested using Student's t test or one-way or two-way ANOVA as indicated in the figure legends, using Graphpad Prism software. Post-test corrections are indicated in the legends. Differences were considered statistically significant if $p < 0.05$ using FDR corrections for multiple testing where applicable.

DATA AVAILABILITY

Data are available from the corresponding authors on reasonable request. RNA-seq data are deposited at the GEO repository under accession number GEO: GSE235940.

SUPPLEMENTAL INFORMATION

Supplemental information can be found online at https://doi.org/10.1016/j.ymthe.2023.06.020.

ACKNOWLEDGMENTS

We thank Luke Harrison for the creation of the graphical abstract and help with text editing, Raúl Terrón Expósito and Daniela Hass for technical assistance, and Anja Zeigerer for help with microscopy. We thank Ez-Zoubir Amri for the hMADSCs. The graphical abstract was created with BioRender.com. Molecular graphics and analyses performed with UCSF ChimeraX, developed by the Resource for Biocomputing, Visualization, and Informatics at the University of California, San Francisco, with support from National Institutes of Health R01-GM129325 and the Office of Cyber Infrastructure and Computational Biology, National Institute of Allergy and Infectious Diseases. M.G. was supported by an Alexander von Humboldt Foundation postdoctoral fellowship. M.R. is funded by the European Research Council (ERC) under the European Union's Horizon 2020 research and innovation program (# 949017) and Helmholtz Association - Initiative and Networking Fund.

AUTHOR CONTRIBUTIONS

Conceptualization, O.P., S.H., and M.R.; data curation and formal analysis, H.J., F.E., P.M., M.G., S.B., P.G., J.S., M.B.D., and M.R.; investigation and methodology, H.J., F.E., and M.R.; visualization, H.J., F.E., S.B., and M.R.; writing – original draft, H.J. and M.R.; writing – review & editing, H.J., F.E., S.B., J.S., O.P., S.H., and M.R.

DECLARATION OF INTERESTS

This work was in part supported by research grants by Novo Nordisk to O.P., S.H., and M.R.

REFERENCES

1. Argilés, J.M., Stemmler, B., López-Soriano, F.J., and Busquets, S. (2019). Inter-tissue communication in cancer cachexia. Nat. Rev. Endocrinol. *15*, 9–20. https://doi.org/10.1038/s41574-018-0123-0.

2. Deans, D.A.C., Tan, B.H., Wigmore, S.J., Ross, J.A., de Beaux, A.C., Paterson-Brown, S., and Fearon, K.C.H. (2009). The influence of systemic inflammation, dietary intake and stage of disease on rate of weight loss in patients with gastro-oesophageal cancer. Br. J. Cancer *100*, 63–69. https://doi.org/10.1038/sj.bjc.6604828.

3. Kalantar-Zadeh, K., Rhee, C., Sim, J.J., Stenvinkel, P., Anker, S.D., and Kovesdy, C.P. (2013). Why cachexia kills: examining the causality of poor outcomes in wasting conditions. J. Cachexia Sarcopenia Muscle *4*, 89–94. https://doi.org/10.1007/s13539-013-0111-0.

4. Warren, S. (1932). The immediate causes of death in cancer. Am. J. Med. Sci. *184*, 610–615. https://doi.org/10.1097/00000441-193211000-00002.

5. Vegiopoulos, A., Rohm, M., and Herzig, S. (2017). Adipose tissue: between the extremes. EMBO J. *36*, 1999–2017. https://doi.org/10.15252/embj.201696206.

6. Fullerton, M.D., Galic, S., Marcinko, K., Sikkema, S., Pulinilkunnil, T., Chen, Z.-P., O'Neill, H.M., Ford, R.J., Palanivel, R., O'Brien, M., et al. (2013). Single phosphorylation sites in Acc1 and Acc2 regulate lipid homeostasis and the insulin-sensitizing effects of metformin. Nat. Med. *19*, 1649–1654. https://doi.org/10.1038/nm.3372.

7. Dzamko, N., van Denderen, B.J.W., Hevener, A.L., Jørgensen, S.B., Honeyman, J., Galic, S., Chen, Z.-P., Watt, M.J., Campbell, D.J., Steinberg, G.R., and Kemp, B.E. (2010). AMPK beta1 deletion reduces appetite, preventing obesity and hepatic insulin resistance. J. Biol. Chem. *285*, 115–122. https://doi.org/10.1074/jbc.M109.056762.

8. Gaidhu, M.P., Bikopoulos, G., and Ceddia, R.B. (2012). Chronic AICAR-induced AMP-kinase activation regulates adipocyte lipolysis in a time-dependent and fat depot-specific manner in rats. Am. J. Physiol. Cell Physiol. *303*, C1192–C1197. https://doi.org/10.1152/ajpcell.00159.2012.

9. Daval, M., Diot-Dupuy, F., Bazin, R., Hainault, I., Viollet, B., Vaulont, S., Hajduch, E., Ferré, P., and Foufelle, F. (2005). Anti-lipolytic Action of AMP-activated Protein Kinase in Rodent Adipocytes. J. Biol. Chem. *280*, 25250–25257. https://doi.org/10.1074/jbc.M414222200.

10. Djouder, N., Tuerk, R.D., Suter, M., Salvioni, P., Thali, R.F., Scholz, R., Vaahtomeri, K., Auchli, Y., Rechsteiner, H., Brunisholz, R.A., et al. (2010). PKA phosphorylates

and inactivates AMPKα to promote efficient lipolysis. EMBO J. *29*, 469–481. https://doi.org/10.1038/emboj.2009.339.

11. Boon, H., Bosselaar, M., Praet, S.F.E., Blaak, E.E., Saris, W.H.M., Wagenmakers, A.J.M., McGee, S.L., Tack, C.J., Smits, P., Hargreaves, M., and van Loon, L.J.C. (2008). Intravenous AICAR administration reduces hepatic glucose output and inhibits whole body lipolysis in type 2 diabetic patients. Diabetologia *51*, 1893–1900. https://doi.org/10.1007/s00125-008-1108-7.

12. Steinberg, G.R., and Carling, D. (2019). AMP-activated protein kinase: the current landscape for drug development. Nat. Rev. Drug Discov. *18*, 527–551. https://doi.org/10.1038/s41573-019-0019-2.

13. Bourron, O., Daval, M., Hainault, I., Hajduch, E., Servant, J.M., Gautier, J.F., Ferré, P., and Foufelle, F. (2010). Biguanides and thiazolidinediones inhibit stimulated lipolysis in human adipocytes through activation of AMP-activated protein kinase. Diabetologia *53*, 768–778. https://doi.org/10.1007/s00125-009-1639-6.

14. Qi, J., Gong, J., Zhao, T., Zhao, J., Lam, P., Ye, J., Li, J.Z., Wu, J., Zhou, H.-M., and Li, P. (2008). Downregulation of AMP-activated protein kinase by Cidea-mediated ubiquitination and degradation in brown adipose tissue. EMBO J. *27*, 1537–1548. https://doi.org/10.1038/emboj.2008.92.

15. Rohm, M., Schäfer, M., Laurent, V., Üstünel, B.E., Niopek, K., Algire, C., Hautzinger, O., Sijmonsma, T.P., Zota, A., Medrikova, D., et al. (2016). An AMP-activated protein kinase–stabilizing peptide ameliorates adipose tissue wasting in cancer cachexia in mice. Nat. Med. *22*, 1120–1130. https://doi.org/10.1038/nm.4171.

16. Copolovici, D.M., Langel, K., Eriste, E., and Langel, Ü. (2014). Cell-Penetrating Peptides: Design, Synthesis, and Applications. ACS Nano *8*, 1972–1994. https://doi.org/10.1021/nn4057269.

17. Xie, J., Bi, Y., Zhang, H., Dong, S., Teng, L., Lee, R.J., and Yang, Z. (2020). Cell-Penetrating Peptides in Diagnosis and Treatment of Human Diseases: From Preclinical Research to Clinical Application. Front. Pharmacol. *11*, 697. https://doi.org/10.3389/fphar.2020.00697.

18. Wang, F., Wang, Y., Zhang, X., Zhang, W., Guo, S., and Jin, F. (2014). Recent progress of cell-penetrating peptides as new carriers for intracellular cargo delivery. J. Control Release *174*, 126–136. https://doi.org/10.1016/j.jconrel.2013.11.020.

19. Gomez, J.A., Chen, J., Ngo, J., Hajkova, D., Yeh, I.-J., Gama, V., Miyagi, M., and Matsuyama, S. (2010). Cell-Penetrating Penta-Peptides (CPP5s): Measurement of Cell Entry and Protein-Transduction Activity. Pharmaceuticals *3*, 3594–3613. https://doi.org/10.3390/ph3123594.

20. Derossi, D., Joliot, A.H., Chassaing, G., and Prochiantz, A. (1994). The third helix of the Antennapedia homeodomain translocates through biological membranes. J. Biol. Chem. *269*, 10444–10450.

21. Nakayama, F., Yasuda, T., Umeda, S., Asada, M., Imamura, T., Meineke, V., and Akashi, M. (2011). Fibroblast growth factor-12 (FGF12) translocation into intestinal epithelial cells is dependent on a novel cell-penetrating peptide domain: involvement of internalization in the in vivo role of exogenous FGF12. J. Biol. Chem. *286*, 25823–25834. https://doi.org/10.1074/jbc.M110.198267.

22. Gautam, A., Chaudhary, K., Kumar, R., Sharma, A., Kapoor, P., Tyagi, A., and Raghava, G.P.S.; Open source drug discovery consortium (2013). In silico approaches for designing highly effective cell penetrating peptides. J. Transl. Med. *11*, 74. https://doi.org/10.1186/1479-5876-11-74.

23. Myers, R.W., Guan, H.-P., Ehrhart, J., Petrov, A., Prahalada, S., Tozzo, E., Yang, X., Kurtz, M.M., Trujillo, M., Gonzalez Trotter, D., et al. (2017). Systemic pan-AMPK activator MK-8722 improves glucose homeostasis but induces cardiac hypertrophy. Science *357*, 507–511. https://doi.org/10.1126/science.aah5582.

24. Christ-Crain, M., Kola, B., Lolli, F., Fekete, C., Seboek, D., Wittmann, G., Feltrin, D., Igreja, S.C., Ajodha, S., Harvey-White, J., et al. (2008). AMP-activated protein kinase mediates glucocorticoid- induced metabolic changes: a novel mechanism in Cushing's syndrome. FASEB J. *22*, 1672–1683. https://doi.org/10.1096/fj.07-094144.

25. Inoue, E., and Yamauchi, J. (2006). AMP-activated protein kinase regulates PEPCK gene expression by direct phosphorylation of a novel zinc finger transcription factor. Biochem. Biophys. Res. Commun. *351*, 793–799. https://doi.org/10.1016/j.bbrc.2006.10.124.

26. McGee, S.L., van Denderen, B.J.W., Howlett, K.F., Mollica, J., Schertzer, J.D., Kemp, B.E., and Hargreaves, M. (2008). AMP-Activated Protein Kinase Regulates GLUT4 Transcription by Phosphorylating Histone Deacetylase 5. Diabetes *57*, 860–867. https://doi.org/10.2337/db07-0843.

27. Sukari, A., Muqbil, I., Mohammad, R.M., Philip, P.A., and Azmi, A.S. (2016). F-BOX proteins in cancer cachexia and muscle wasting: Emerging regulators and therapeutic opportunities. Semin. Cancer Biol. *36*, 95–104. https://doi.org/10.1016/j.semcancer.2016.01.002.

28. Das, S.K., Eder, S., Schauer, S., Diwoky, C., Temmel, H., Guertl, B., Gorkiewicz, G., Tamilarasan, K.P., Kumari, P., Trauner, M., et al. (2011). Adipose Triglyceride Lipase Contributes to Cancer-Associated Cachexia. Science *333*, 233–238. https://doi.org/10.1126/science.1198973.

29. Sullivan, J.E., Brocklehurst, K.J., Marley, A.E., Carey, F., Carling, D., and Beri, R.K. (1994). Inhibition of lipolysis and lipogenesis in isolated rat adipocytes with AICAR, a cell-permeable activator of AMP-activated protein kinase. FEBS Lett. *353*, 33–36. https://doi.org/10.1016/0014-5793(94)01006-4.

30. Steinberg, G.R., and Hardie, D.G. (2023). New insights into activation and function of the AMPK. Nat. Rev. Mol. Cell Biol. *24*, 255–272. https://doi.org/10.1038/s41580-022-00547-x.

31. Laurencikiene, J., Stenson, B.M., Arvidsson Nordström, E., Agustsson, T., Langin, D., Isaksson, B., Permert, J., Rydén, M., and Arner, P. (2008). Evidence for an Important Role of CIDEA in Human Cancer Cachexia. Cancer Res. *68*, 9247–9254. https://doi.org/10.1158/0008-5472.CAN-08-1343.

32. Morigny, P., Zuber, J., Haid, M., Kaltenecker, D., Riols, F., Lima, J.D.C., Simoes, E., Otoch, J.P., Schmidt, S.F., Herzig, S., et al. (2020). High levels of modified ceramides are a defining feature of murine and human cancer cachexia. J. Cachexia Sarcopenia Muscle *11*, 1459–1475. https://doi.org/10.1002/jcsm.12626.

33. Fearon, K., Strasser, F., Anker, S.D., Bosaeus, I., Bruera, E., Fainsinger, R.L., Jatoi, A., Loprinzi, C., MacDonald, N., Mantovani, G., et al. (2011). Definition and classification of cancer cachexia: an international consensus. Lancet Oncol. *12*, 489–495. https://doi.org/10.1016/S1470-2045(10)70218-7.

34. Schmidt, S.F., Rohm, M., Herzig, S., and Berriel Diaz, M. (2018). Cancer Cachexia: More Than Skeletal Muscle Wasting. Trends Cancer *4*, 849–860. https://doi.org/10.1016/j.trecan.2018.10.001.

35. Baracos, V.E., Martin, L., Korc, M., Guttridge, D.C., and Fearon, K.C.H. (2018). Cancer-associated cachexia. Nat. Rev. Dis. Primers *4*, 17105. https://doi.org/10.1038/nrdp.2017.105.

36. Agustsson, T., Rydén, M., Hoffstedt, J., van Harmelen, V., Dicker, A., Laurencikiene, J., Isaksson, B., Permert, J., and Arner, P. (2007). Mechanism of Increased Lipolysis in Cancer Cachexia. Cancer Res. *67*, 5531–5537. https://doi.org/10.1158/0008-5472.CAN-06-4585.

37. Fouladiun, M., Körner, U., Bosaeus, I., Daneryd, P., Hyltander, A., and Lundholm, K.G. (2005). Body composition and time course changes in regional distribution of fat and lean tissue in unselected cancer patients on palliative care–correlations with food intake, metabolism, exercise capacity, and hormones. Cancer *103*, 2189–2198. https://doi.org/10.1002/cncr.21013.

38. Al-Sawaf, O., Weiss, J., Skrzypski, M., Lam, J.M., Karasaki, T., Zambrana, F., Kidd, A.C., Frankell, A.M., Watkins, T.B.K., Martínez-Ruiz, C., et al. (2023). Body composition and lung cancer-associated cachexia in TRACERx. Nat. Med. *29*, 846–858. https://doi.org/10.1038/s41591-023-02232-8.

39. Kays, J.K., Shahda, S., Stanley, M., Bell, T.M., O'Neill, B.H., Kohli, M.D., Couch, M.E., Koniaris, L.G., and Zimmers, T.A. (2018). Three cachexia phenotypes and the impact of fat-only loss on survival in FOLFIRINOX therapy for pancreatic cancer. J. Cachexia Sarcopenia Muscle *9*, 673–684. https://doi.org/10.1002/jcsm.12307.

40. Reddel, C.J., Allen, J.D., Ehteda, A., Taylor, R., Chen, V.M.Y., Curnow, J.L., Kritharides, L., and Robertson, G. (2017). Increased thrombin generation in a mouse model of cancer cachexia is partially interleukin-6 dependent. J. Thromb. Haemost. *15*, 477–486. https://doi.org/10.1111/jth.13612.

41. Prawitt, J., Niemeier, A., Kassem, M., Beisiegel, U., and Heeren, J. (2008). Characterization of lipid metabolism in insulin-sensitive adipocytes differentiated from immortalized human mesenchymal stem cells. Exp. Cell Res. *314*, 814–824. https://doi.org/10.1016/j.yexcr.2007.11.011.

42. Giroud, M., Tsokanos, F.-F., Caratti, G., Kotschi, S., Khani, S., Jouffe, C., Vogl, E.S., Irmler, M., Glantschnig, C., Gil-Lozano, M., et al. (2021). HAND2 is a novel

obesity-linked adipogenic transcription factor regulated by glucocorticoid signalling. Diabetologia *64*, 1850–1865. https://doi.org/10.1007/s00125-021-05470-y.

43. Rodriguez, A.-M., Elabd, C., Delteil, F., Astier, J., Vernochet, C., Saint-Marc, P., Guesnet, J., Guezennec, A., Amri, E.-Z., Dani, C., and Ailhaud, G. (2004). Adipocyte differentiation of multipotent cells established from human adipose tissue. Biochem. Biophys. Res. Commun. *315*, 255–263. https://doi.org/10.1016/j.bbrc.2004.01.053.

44. Pettersen, E.F., Goddard, T.D., Huang, C.C., Meng, E.C., Couch, G.S., Croll, T.I., Morris, J.H., and Ferrin, T.E. (2021). UCSF ChimeraX: Structure visualization for researchers, educators, and developers. Protein Sci. *30*, 70–82. https://doi.org/10.1002/pro.3943.